

Curvature Attribute from Surface-Restoration as Predictor Variable in Kupferschiefer Copper Potentials

An Example from the Fore-Sudetic Region

Pablo Mejía-Herrera,^{1,2} Jean-Jacques Royer,¹ Guillaume Caumon,¹ and Alain Cheilletz¹

Received 30 March 2014; accepted 20 June 2014
Published online: 2 August 2014

This work explains a procedure to predict Cu potentials in the ore-Kupferschiefer using structural surface-restoration and logistic regression (LR) analysis. The predictor in the assessments are established from the restored horizon that contains the ore-series. Applying flexural-slip to unfold/unfault the 3D model of the Fore-Sudetic Monocline, we obtained curvature for each restored time. We found that curvature represents one of the main structural features related to the Cu mineralization. Maximum curvature corresponds to high internal deformation in the restored layers, evidencing faulting and damaged areas in the 3D model. Thus, curvature may highlight fault systems that drove fluid circulation from the basement and host the early mineralization stages. In the Cu potential modeling, curvature, distance to the Fore-Sudetic Block and depth of restored Zechstein at Cretaceous time are used as predictors and proven Cu-potential areas as targets. Then, we applied LR analysis establishing the separating function between mineralized and non-mineralized locations. The LR models show positive correspondence between predicted probabilities of Cu-potentials and curvature estimated on the surface depicting the mineralized layer. Nevertheless, predicted probabilities are particularly higher using curvatures obtained from Late Paleozoic and Late Triassic restorations.

KEY WORDS: Structural restoration, Fault system, Fault activity, Logistic regression, Predictive modeling.

INTRODUCTION

Fault systems in the basement have played a major role during the genesis of the Poland Kupferschiefer deposit (Fig. 1). First, these structures have driven fluid migration from brines in deeper parts of bedrock (Jowett 1986; Blundell et al. 2003;

Muchez et al. 2005; Wedepohl and Rentzsch 2006; Hitzman et al. 2010). Second, relative high permeability and porosity, required for circulation and accumulation of metals during mineralization, occurred near to basement fault systems (Forster and Smith 1989; Rentzsch et al. 1997; Wagner et al. 2010). Rentzsch and Franzke (1997) have shown several examples of close relationship between major tectonic structures and Kupferschiefer ores in central Germany. To identify the fault systems related to Kupferschiefer-ore locations is an important issue in present day exploration campaigns. However, to recognize these ore-controlling structures sometimes requires huge cost surveys. A first

¹Université de Lorraine-ENSG, CNRS-CREGU, Géoressources, UMR 7359, 2 rue du doyen Marcel Roubault, TSA 70605 54518, Vandoeuvre-lès-Nancy Cedex, France.

²To whom correspondence should be addressed; e-mail: mejia.pablo@gmail.com

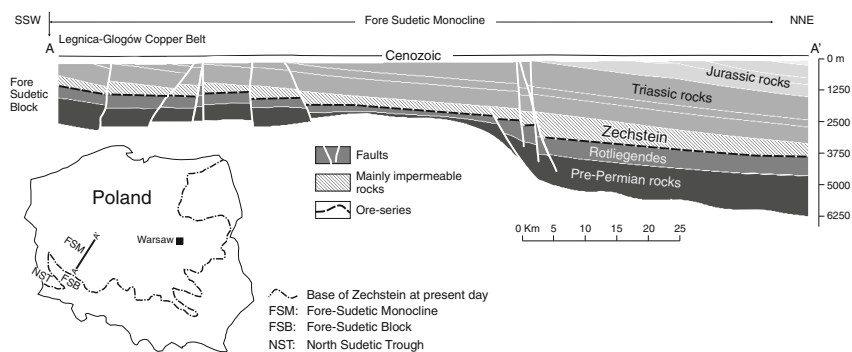


Fig. 1. Simplified geological cross section across the Fore-Sudetic Monocline.

exploration challenge is that buried basement faults are not easily detected, or subject to uncertainty inherent to data interpretation (Lecour et al. 2001; Bond et al. 2007). A second challenge is due to deformation (folding and faulting developed during the structural evolution), which can blur links between a given mineralized location and its corresponding basement fault system. Indeed, fault activity may vary through time and space, with possibly strong impact on rock permeability and mineralized fluid circulation. Even in cases where fault systems are identified, it is necessary to establish their role and timing of activity to understand their role for a given mineralized locality. To overcome this, we propose to use curvature values obtained from a sequential surface-restoration process for inferring the existence and activity of basement-faults related to Cu mineralization. Curvature, as geometric attribute measurable in horizons of a surface-structural model, can reveal internal deformation in those horizons due a faulting event (Mallet 2002; Moretti et al. 2007). Curvature, computed after several sequential restorations, can be translated as the signal of basement faults presence and also indicates their activity over the geologic record. Estimating correlation between curvature and mineralized locations, it is possible to deduce fault-fractures linked to Kupferschiefer-ores. Finally, we evaluated the usefulness of curvatures as a predictor in the Fore-Sudetic Monocline (FSM), SW of Poland, with the application of a multivariate data-driven predictive method. Particularly, we chose logistic regression (LR) analysis to obtain a predictive model as a combination of curvatures acquired in the restorations. The results show that in locations with high curvature values the predicted probability to host a Cu mineralization increases considerably. We suggest that this methodology provides useful evi-

dence for the Cu potentials assessments in the FSM region.

GENERAL GEOLOGY

The Kupferschiefer is a metal-bearing black shale, broadly spread across central Europe (from Ireland to Belarus), with very well-known high Cu-grade locations in SW Poland and central Germany (Rentzsch and Franzke 1997; Oszczepalski and Speczik 2011). The Kupferschiefer-ore exploitation in the Legnica-Głogów Copper Belt Area (LGCB), located within the FSM, is one of most important sources of Cu and Ag in the world (KGHM Polska Miedź 2012). This layer was formed at the end of the Permian, overlying volcanoclastic sequences (Rotliegendes and Wessliegendes) of Saxonian age (Oszczepalski 1999), and overlain by sedimentary products (mainly evaporites) of eustatic variations during the Guadalupian to Lopingian (Zechstein Formation) (Lefebvre 1989).

Geologic Settings of the FSM

The Kupferschiefer Formation overlies a group of Early Permian sub-basins covering Paleozoic rocks affected by Caledonian and Variscan tectonics (Karnkowski 1999). The post-Permian sediments correspond to continental successions and shallow marine sediments of Triassic age followed by a Jurassic succession of shallow marine sediments. Basin analysis shows subsidence rates in the Late Permian-Early Triassic superiors to 80 m/m.y. (Central Basin) (Karnkowski 1999; Resak et al. 2008). This rate decreased substantially in Late Triassic and is

maintained through to the Jurassic (Karnkowski 1999). At the end of the Jurassic, the top Rotliegend surface in the Lower Silesian basin was at a depth of up to 4 km (Blundell et al. 2003). At the Jurassic–Cretaceous boundary, the Lower Silesian basin was inverted and uplifted, creating the Fore-Sudetic block, bounded by NW-SE trending faults extending from the basement to the post-Permian successions (Blundell et al. 2003). The Cretaceous sediments, present in the eastern part of the Fore-Sudetic Monocline, comprise mainly of sandstones, conglomerates and marls. These rocks unconformably cover older strata (Pieczonka et al. 2008). Northern-Europe was affected by a Late Cretaceous–Early Paleocene tectonic inversion, probably linked to an early Alpine orogeny phase. This event produced the most intensive tectonic movements in the Fore–Sudetic Monocline (Pieczonka et al. 2008), provoking the erosion of hundreds to thousands meters of sediments (Mazur et al. 2005; Scheck-Wenderoth and Lamarche 2005; Resak et al. 2008; Narkiewicz et al. 2010). In the Lubin region, the uplift is estimated to be >1,000 m (Stephenson et al. 2003), eroding rocks from Triassic to Cretaceous. The pre-Cenozoic rocks were tilted 3°–6° to the NE, probably during the Alpine orogeny. The post-Variscan cover of Permian–Cenozoic formations is subdivided into the Kimmerian (Permian, Triassic, Jurassic), Laramide (Cretaceous), and post-Laramide stages (Tertiary, Quaternary) (Oszczepalski 1999).

Mineralization

Three main mineralized sulfide levels both as grains and veinlets can be identified within the shales: a lower dolomite level, an intermediate bituminous black shale level and an upper dolomite black shale level. The main minerals in the polymetallic Kupferschiefer ore in the Fore-Sudetic area are Cu(Cu-Ag) sulfides and other mineral species such as arsenides, sulphosalts, thiosulfates, arsenates and precious metals (Oszczepalski 1999; Piestrzyński et al. 2002). At least three stages are involved in the ore-Kupferschiefer formation (Vaughan et al. 1989; Wodzicki and Piestrzyński 1994; Speczik 1995; Wagner et al. 2010), which represent broadly the main post-Permian tectono-magmatic events in central Europe (Schmidt Mumm and Wolfgramm 2004). The first stage is associated with diagenesis during a Triassic to Early Jurassic rifting event (Ziegler 1982; Bechtel et al. 1999). A second stage is

related to the Late Jurassic extensional tectonic event that formed the nearby North German Basin, reactivating Variscan basement faults and extending them upwards through the overlying strata (Symons et al. 2011). Finally, basin inversion and uplifting occurred in northern Europe in the Late Cretaceous–Early Paleocene. This led to erosion of several hundred meters of the Triassic to Cretaceous sedimentary formations (Resak et al. 2008). This last erosion event likely provoked increase of fluid/lithostatic pressure ratio, and hydraulic fracturing allowing circulation of mineralizing fluids, remobilization of elements and replacement and enrichment of Cu-sulfides (Mejia and Royer 2012).

MODELING THE FORE-SUDETIC MONOCLINE

Modeling Outlines

The surface-based modeling of the FSM is established on cartographic and interpreted subsurface data, which were integrated in a *SKUA -2011* framework, resulting in a consistent model that honors the input data. The management of data and the main model-building tasks were realized as suggested by Caumon et al. (2009) and PARADIGM (2012). The topographic information was obtained from the SRTM 90m digital elevation data freely provided by the International Centre for Tropical Agriculture (Jarvis et al. 2008). The subsurface data were introduced picking the lithological contacts and faults from regional cartographic information (Dadlez et al. 2000; Pawlak et al. 2008; Oszczepalski and Speczik 2011). Interpreted cross-section from wells and seismic surveys (Wodzicki and Piestrzyński 1994; Krzywiec 2006; Mazur et al. 2010) were used to establish thicknesses and shapes of the main rock units (Fig. 2).

Outcome FSM 3D Model

The resulting model covers a surface of >31,000 km² extending from the Fore-Sudetic Block to Świebodzin at north and Kluczbork at east. The vertical extension is down to 6.3 Km *mbsl* in the deepest part. The grid resolution used in the implicit modeling was about 2 km and 0.5 km horizontally and vertically, respectively. 17 horizons from Cenozoic to the top of Precambrian rocks were created, corresponding to five main

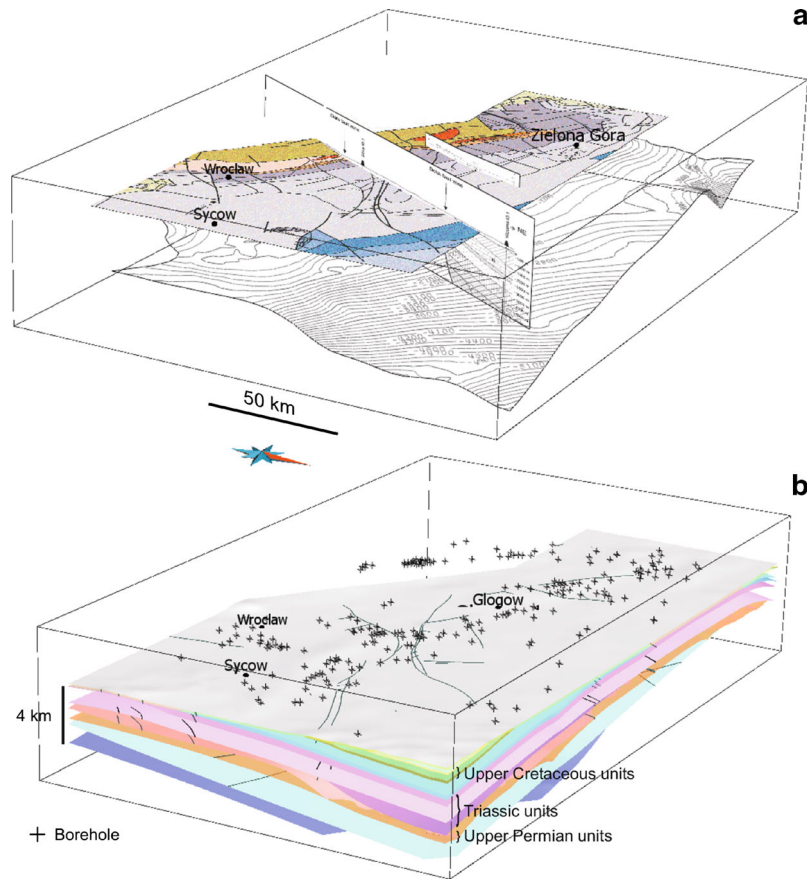


Fig. 2. Fore-Sudetic Monocline 3D model built using the *structure and stratigraphy SKUA -2011* workflow. a The input data comprise cross-sections, a regional geological map of the study area and the interpolated Kupferschiefer depth. The contacts and unit limits are introduced by picking both the map and the cross-sections (see Sect. 3.1). b The meshed domain necessary for the implicit modeling has a resolution of 2,000 and 500 m horizontal and vertical, respectively. The sedimentary units overlaying the pre-Triassic rocks are considered as conformable in the *structure and stratigraphy* workflow, except for the Post-Cretaceous units deposited upon the eroded Upper Cretaceous units. The Upper Permian units are considered deposited in baselap mode. The crosses represent the borehole locations from Oszczepalski et al. (1997).

depositional periods: Upper Permian to Triassic, Triassic, Jurassic, Cretaceous, and Oligocene to present day. The geometry of the FSM consists of gently NE-dipping strata except for the sub-horizontal Cenozoic units. In general, the final model is similar to an inclined layer cake horizontally eroded in the upper part, lightly folded in the central region with a NE strike fold axis (Fig. 3). Finally, we extracted surfaces representing the top of the main sedimentary units namely: pre-Rotliegend, Rotliegend, Zechstein, Triassic, Jurassic, erosion Cretaceous-Paleocene and post-Oligocene. The top

of the Cretaceous (now eroded) was extrapolated following the shape and morphology of the preserved units.

DETECTING FAULT ACTIVITY FROM RESTORATION

Restoration Goals

Restoration aims at reconstructing the original geometry from the current structural geometry. For

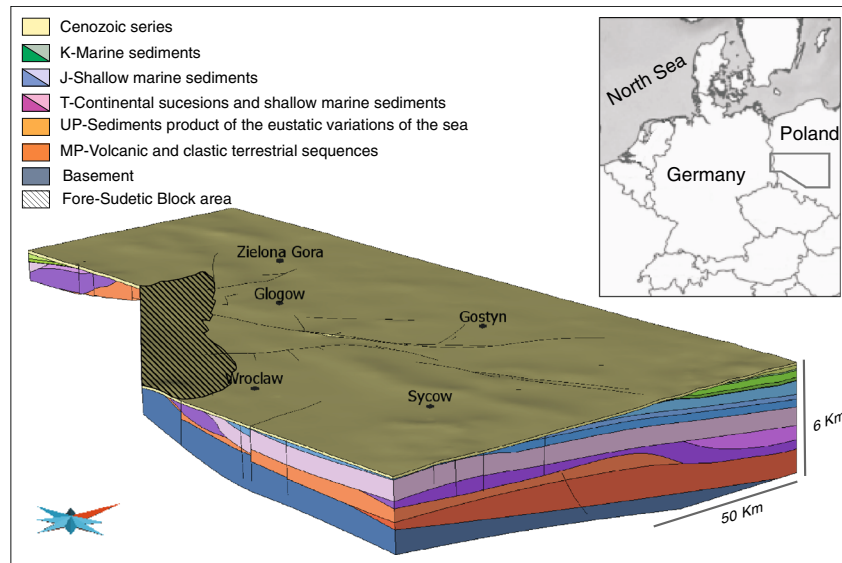


Fig. 3. Location of the study area and resulting model of the FSM.

example, in deformed sedimentary rocks restoration is used to find the original depositional state at a given time. The first attempts to restore a starting geometry were conducted more than 100 years ago by Chamberlin (1910) using an areal preservation criterion in cross-section analysis. Later, his concepts were extended in a volume constant criterion in foreland compressive belts by Dahlstrom (1969). In the last decade, restoration methods integrating the mechanical properties of rocks have been proposed (De Santi et al. 2002; Maerten and Maerten 2006; Moretti et al. 2006; Moretti 2008; Guzowski et al. 2009; Durand-Riard et al. 2013). Although it is proved that accounting for rock mechanic parameters in the restoration offers greater precision and provides better accuracy for describing strain and stress fields (Durand-Riard et al. 2010; Vidal-Royo et al. 2012; Durand-Riard et al. 2013), 3D conformable mesh generation is a significant challenge at large scale. Mesh generation is often time-consuming and requires a very large number of elements to honor fine-scale structural features, especially in complex faulted contexts (Moretti 2008; Caumon 2010; Durand-Riard et al. 2010; Botella et al. 2013). Thus, in this work, we use simple geometric analysis to restore layers to their original depositional states applying surface restoration (also called 2.5D restoration). In the next sections, we explain the basis and methods of 2.5D structural

restoration, focusing on detecting faults presence and estimating their activity.

Surface Restoration

The aim of 2.5D restoration is to remove fault slip and unfold deformed surfaces. The unfauling aims at matching horizon cutoff lines on either side of a fault that compound a given surface. The simplest unfauling procedure consists in a rigid-body displacement, generally accomplished by domino-block and circular-fault methods (Rouby 1994; Groshong 2006). The unfolding aims to flatten a surface, considering that the continuous part of a surface can return to its original geometry following one of these methods: (i) *Simple-shear* slip on closely spaced parallel planes (Verrall 1981); (ii) *Flexural slip* slip parallel to bedding (Dahlstrom 1969).

Because these concepts were initially defined in cross-sections, their applications to map restorations of faulted, and possibly non-developable surfaces, call for specific algorithms, among which are *triangle adjustment* (Gratier and Guillier 1993), *extrapolation of parallel cross-sections* (Moretti et al. 2007) and *parameterization* (Mallet 2002; Moretti 2008). In this work we applied *flexural slip*, which is achieved by *parameterization*, preserving the global area of folded and restored surfaces.

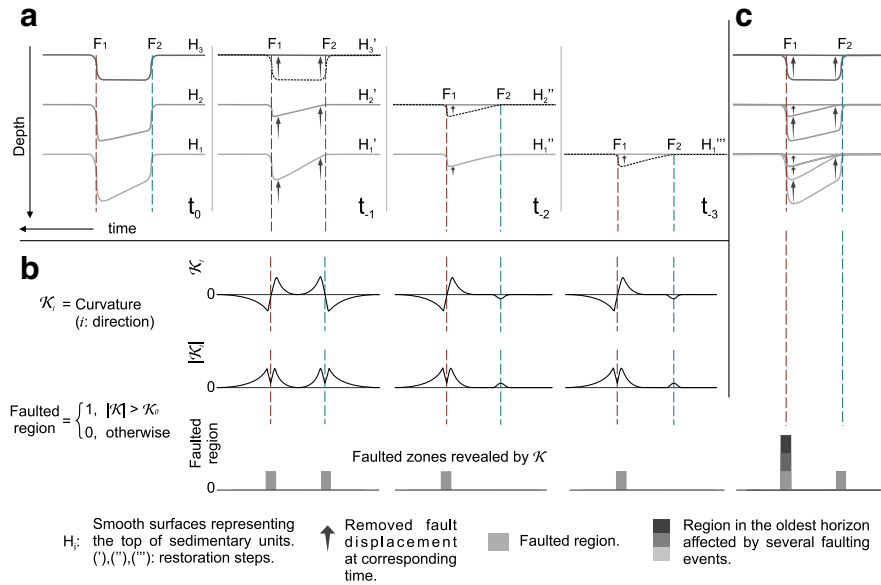


Fig. 4. a Schematic surface-restoration workflow. The flattening of the upper surface removes the deformation caused by fault activity at the corresponding time. This flattening is propagated on the underlying surfaces. b The curvature, obtained at each restoration, is higher in the folded neighborhood than in the rest of the surface. c For the overall restoration process, the regions affected by several faulting events are highlighted by high curvature values. In this example, the fault F_1 has been active for a longer period than F_2 .

Iterative Restoration

In sequential-surface restoration, the horizons are restored iteratively from top to bottom. When a horizon is restored, the deformation is propagated to the underlying horizons (Mallet 2002). This implies that two parallel horizons are flattened at once when restoring the upper horizon only. If this is not the case, it probably means that a deformation event (or several) occurred before the deposition of the layer represented by the upper surface (Fig. 4a). After removing the upper restored reference surface and decompacting the entire stack of sediments using an isostatic approach (Sclater and Christie 1980), which is called back-stripping, sequential, deterministic, surface restoration is applied to simulate iteratively from youngest to the oldest sediment layer (Fig. 5a). Although the iterative surface restoration cannot describe the detailed structural evolution of a study area, it is a useful method in the reconstruction of ancient structural stages (Moretti et al. 2007; Titeux 2009).

Internal Deformation and Fault Activity

Although the main restoration aim is to get the original geometry at a given time, other outputs

can be obtained by unfolding and unfauling. Three common outputs correspond to strain, dilation and curvature which account for surface variations between deformed and restored geometry. The strain corresponds to the deformation tensor at each point of the reference surface before and after restoration. In 2.5D restoration, the strain considers only geometric deformation and does not generally reflect mechanical layering. The dilation is trace of strain tensor and corresponds to local area variation between the restored and current geometry. Finally, curvature is a second order tensor defined on the surface. It is a static geometric measure corresponding to the inverse of the radius of all tangent circles orthogonal to the surface. If reversed, the direction in which the radius is smaller corresponds to the maximum curvature, which relates to folding/faulting (Fig. 4b). Assuming surfaces have correct geometry, curvature reveals high deformation zones in horizons (Lisle 1994; Roberts 2001). For each restoration, the curvature analysis on a selected horizon highlights the most deformed regions at the corresponding geologic time. Other attributes from geometric analysis (e.g., curvature gradient using 3D seismic data (Gao 2013)) can express high deformed areas related to faulting.

Continuous-Surface Representation

In this study, horizons were modelled as smoothed-continuous surfaces for two reasons:

Fault uncertainty In the absence of direct fault observations, it could be hazardous to cut horizons with inferred faults. This work aims to correlate mineralization process with fault activity. If we introduce an inferred fault that does not corresponds to the geologic record then the results will be biased. Wrong modeled faults can be the product of bad interpretation, missing data or noise in the raw data (Cherpeau et al. 2010). Instead, it is possible to represent horizons as smoothed continuous surfaces and then use geometric attributes to detect fault activity (see previous section) (Fig. 4c).

Forced-extensional folds Normal extensional faulting in the basement may develop folding in the sedimentary cover (Finch et al. 2004). This is especially observed when a salt layer above the basement introduces a mechanical decoupling between the basement and the overlying rocks (Withjack et al. 1990; Withjack and Callaway 2000). This is the case in the Fore-Sudetic region, where the thick evaporite-rich Zechstein Formation is deposited directly above the basement (see Fig. 1 and Sect. 3). In the FSM, the present day known faults in the cover may correspond to active basement faults. In early to medium stages of the structural evolution of the region, the faulting in the basement could develop forced extensional folding rather than faulting in the above layers. Examples of salt-related folding due to Zechstein presence have been documented in several locations of Europe (Krzywiec 2006; Kane et al. 2010; Duffy et al. 2013). Therefore, we address the problem of detection of fault zones in the basement and their time activity by studying internal deformation in cover horizons depicted as continuous surfaces (Fig. 5b).

Restored Models

The restoration of the FSM is achieved as a multi-sequential surface flattening. Taking as reference the horizon at the top of the stack, unfolding is applied on the hanging wall of this horizon, thus obtaining the field of restoration vectors for this horizon. Then, deformation on the stack is achieved applying the field of restoration vectors on the bottom horizons. Finally, the top layer is removed and the unfolding process starts again (Mallet 2002). We

chose the flexural slip method KINE3D-2, available in *SKUA*, looking for preserving thickness and the global area of the layers. After each restoration, we decompact the sedimentary units applying the methodology suggested by Sclater and Christie (1980). A total of six restoration routines were realized using the KINE3D-2 workflow. During the restoration, some surface inconsistencies (e.g., unrealistic folding, wrong thickness variations, underlying horizons crossing upper horizons) are adjusted manually. In practice, structural restoration is an iterative process which imposes eventually the reconstruction of the initial surface model attempting to correct these inconsistencies. It was achieved by modifying the initial surface shapes honoring the input data. These corrections are performed before making any new restoration operation (Fig. 6).

Restoration Outputs

For each of the five restoration outputs simulating the main depositional phases (Cenozoic, Cretaceous, Jurassic, Triassic and Upper Permian), we obtained the restoration vectors, the strain tensor, the dilation and the curvature. We defined the variable K as the ratio of: the maximum curvature found in the mineralized horizon ($K_{max} = \max(K_i, K_j)$, i, j orthogonal main directions) as positive values ($|K_{max}|$), and the maximum value of $|K_{max}|$ over the surfaces. The more deformed areas are then highlighted as function of the K magnitude between **0** and **1** (Fig. 7).

CURVATURE AND CU ASSESSMENTS

Potentials Assessments and Predictors Variables

In mineral potential modeling, the analytical or empirical relationships between descriptive features and a mineral target express the possibility to predict a given mineral concentration in a location as function of descriptive features (e.g., Quadros et al. 2006; Cheng 2008; Zuo and Carranza 2011; Schaeben 2012). Let evidences denote the set of observed features that are directly related to the mineralization process (e.g., mineral alterations in rocks during a hydrothermal event, or sorting of heavy-minerals grains during a depositional process). Let geo-variables denote the set of features that control the system during mineralization (e.g., pressure, temperature, pH, Eh). Then, in principle, it is possible to

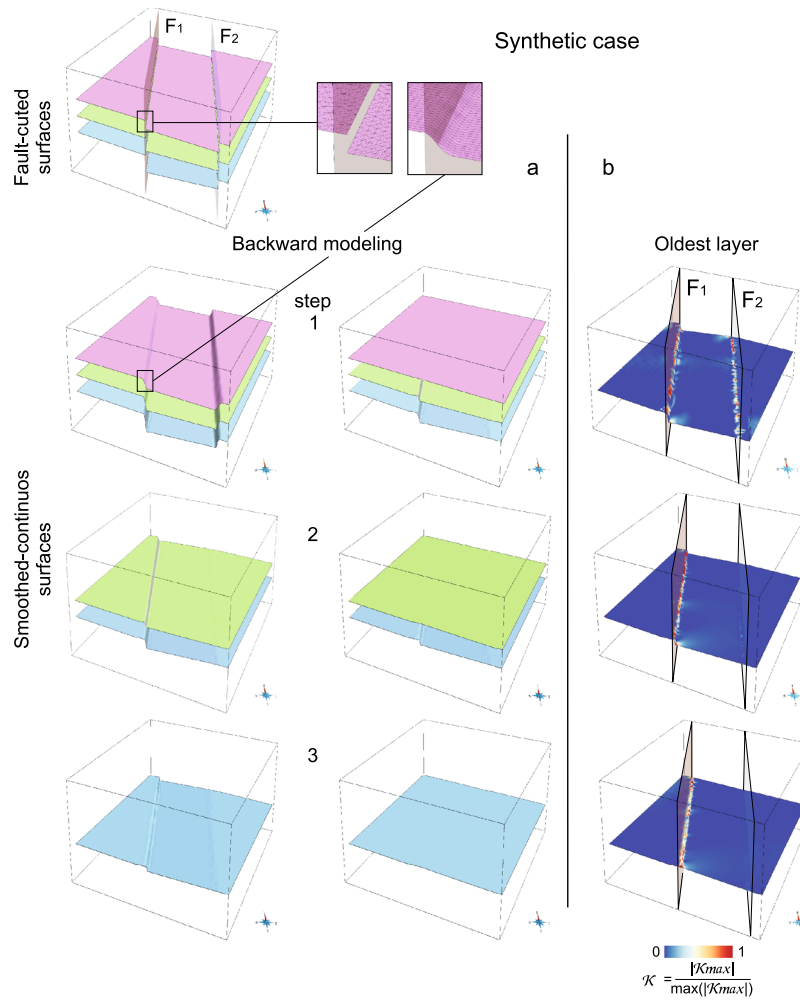


Fig. 5. a Synthetic case of structural restoration. Faulted horizons are represented by smoothed-continuous-triangulated surfaces. After flattening, the upper restored horizon is removed and the restoration process starts again. b The high K_{max} values, stored in the nodes of the oldest layer, reveal the fault activity. Fault F_1 starts its activity before deposition of the middle layer, contrary to F_2 whose activity is evidenced only after deposition of the middle layer.

build a potential model for a given mineralization integrating (as predictors) evidential geo-variables in terms of multivariate statistical analysis (Agterberg et al. 1993; Kerrich 1993; Araújo and Macedo 2002). Several mathematical methods are available to accomplish this, logistic regression (LR) being one of the most employed. Compared to other popular methods (e.g., weight-of-evidence), LR has the advantage of dealing with conditional independence assumptions and works with both continuous and discrete variables (Schaeben 2013, 2014). Specifically, the LR determines a relationship between

the linear combination of predictors and the logit-transformed conditional mean using the logit transform as link function (Eq. 1) (McCullagh and Nelder 1989):

$$\log(Odds) = \beta_0 + \beta_1 x_1 + \beta_2 x_2 + \dots + \beta_m x_m \quad (1)$$

x_{1m} : predictors
 β_{0m} : coefficients

Thus, using curvature as a predictor in LR analysis, it is possible to test the relevance of this restoration output in Cu-potential predictive models.

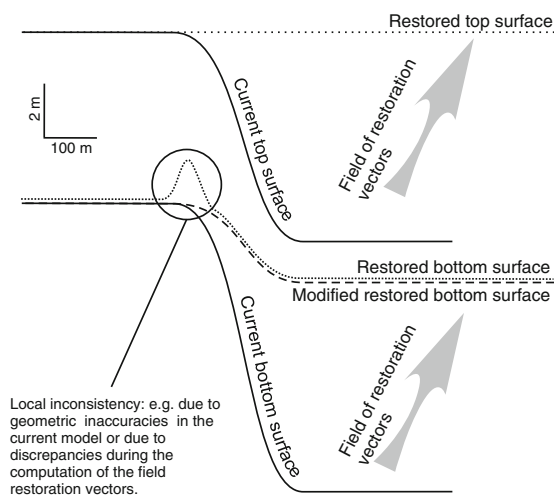


Fig. 6. Cartoon showing some discrepancies that may arise in the unflattened surfaces for a given restoration. These discrepancies are corrected before starting a new restoration routine on the remaining horizons.

Cu Potentials and Selected Predictors

We digitized the Cu-potential areas reported by Oszczepalski and Speczik (2011) in Lower Silesia, including the Legnica–Głogów Copper Belt district. These areas are the result of several exploration programs accounting for more than 370 archival boreholes outside of the LGCB district (Oszczepalski et al. 1997; Speczik et al. 2007). Subsequently, we created a binary attribute of **1** for the highest potentials and **0** for the rest. Then, we generated LR predictive models using the logits of these higher Cu-potentials. The K , estimated in the mineralized horizon after each restoration, is added in the predictive models. Curvature of the top of Cenozoic restoration was not taken into account as it is posterior to the mineralization. Thus, four predictors $K_{l=0:4}$ (l : restoration from Cretaceous to Upper Permian) were integrated in the LR models. Looking to obtain more accurate predictions, we added two other variables in the analysis: horizontal distance from the Fore-Sudetic Block (HFB) and depth of Zechstein base at Late Cretaceous (ZBK), both as continuous predictors. These two attributes were selected among other continuous variables (e.g., distance to current faults, layer thickness, restored depths) due to their good correlation coefficients (0.430 and 0.339, respectively) with the Cu distribution showed by Oszczepalski et al. (1997). The LR models of Cu-potentials per predictor are shown in Tables 1 and 2 and Figure 8.

LR Models by Predictor

The LR models per show that high curvature values, obtained at each restored time, increase the *log Odds* of having a Cu-potential locality (versus not having a Cu-potential locality). These positive coefficients obtained by the K models indicate a positive link between deformation in the horizons, highlighted by curvature, and the Cu-potential zones defined by Oszczepalski and Speczik (2011). Another tendency is observed in relation to the restorations, where the coefficient obtained for K increases by restored time. This trend is observable in Figure 8 where predicted probabilities increase by geologic-time-restoration. In contrast, the negative coefficients for distance HFB and depth ZBK show that the *log Odds* to have a Cu-potential location (versus non Cu-potential) decrease where these variables increase.

Predictive Model and Conditional Independence

Attempting to build a general predictive model of Cu-potentials with the above predictors, we integrated all predictors in a single LR model. Because $K_{(1,2,3,4)}$, HFB and ZBK appear to be mutually dependent conditionally to Cu-potentials (Fig. 9), the interaction terms for them are integrated as predictors trying to yield true conditional probability (Schaeben 2014, 2013; Schaeben and Schmidt 2013). Table 3 shows the LR predictive model integrating all predictors and interaction terms. The resulting LR general model was applied to the study region, thus obtaining the predicted probability map for Cu-potential locations (Fig. 10.)

PERSPECTIVES

High curvature values obtained during all restorations match locally with known mineralized zones. The most important correlations correspond to the present day exploitation area of LGCB, and also in the adjacent Cu-potential locations of Luboszyce, Ścinawa and Ślubów. Other Cu-potential areas that are related to high curvature for all restorations are: Mirków, Sułmierzyce, Czeklin and Kózuchów. The areas of Janowo, Kaleje, and Florentyňa are related to high curvatures in the Upper

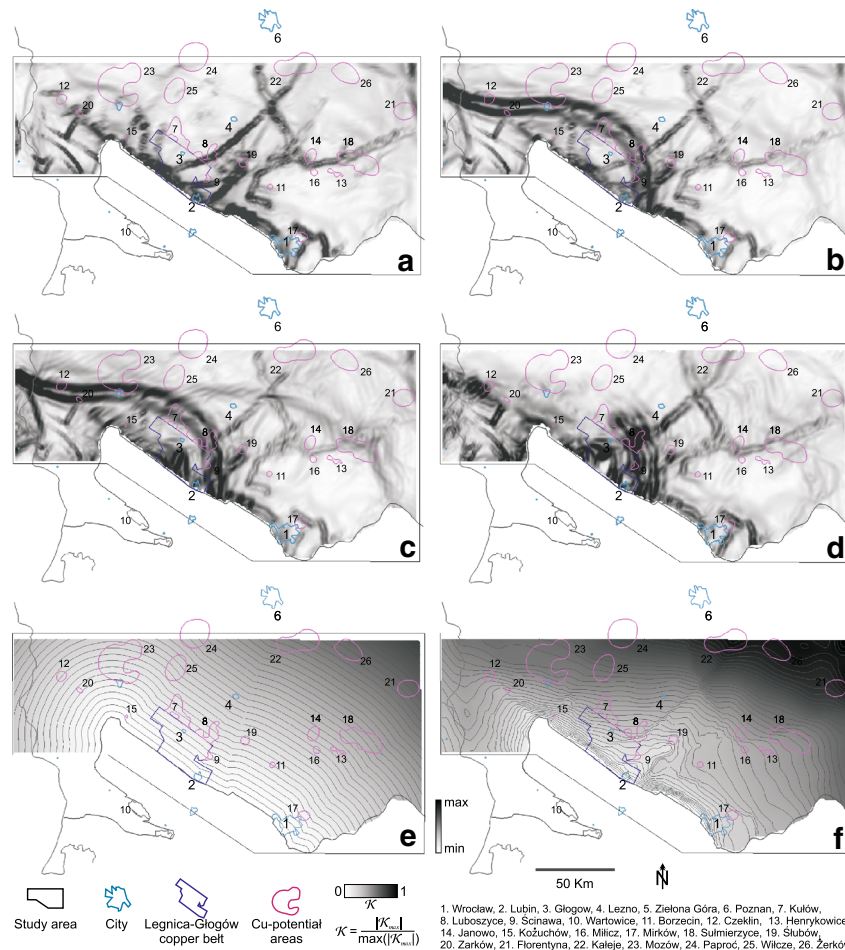


Fig. 7. Maximum curvature corresponding to each restoration from Cretaceous to Upper Permian a Cretaceous, b Jurassic, c Triassic and d Upper Permian. e Horizontal distance to Fore-Sudetic Block. f Depth of the Zechstein base at Late Cretaceous. Some locations related to mining activities are highlighted. Cu-potential areas from Oszczepalski and Speczik (2011) are the result of several exploration programs accounting for more than 370 archival boreholes outside of the LGCB district.

Permian (Top Zechstein) and Cretaceous restored steps. In the Milicz area, good potential may exist in the northern part (Fig. 7).

For the Triassic restoration, the distribution of high curvature values shows strong differences in relation to the Permian restoration. Outside of LGCB, high curvature values are found in the Żary Pericline and Zielona Góra depression. The Cu-potentials areas of Kulów, Wilcze and Zarków appear linked to the increase in curvature values for this restoration step (Fig. 7c). In contrast, Triassic and Jurassic restorations show a similar feature in the obtained curvature, except for the LGCB and Sulmierzyce areas. (Fig. 7b, c). The Cretaceous restoration gives high curvature values on the central

part of the study area and close to the border with the Fore-Sudetic Block. The Paproć and Borzęcin areas present similar curvature values and distribution as in the Jurassic.

In relation with deformation stages, mineralization and Cu-enrichment times, the Odra Fault system may have played a significant role during the Late Permian and Cretaceous at locations such as the LGCB, the north part of the Żary Pericline, and in the Wrocław proximity (Fig. 7d and Fig. 10). In contrast, fault systems associated to the Pogorzela elevation seem to have controlled the Cu mineralization during the Triassic. The Cu-potentials on the Zielona Góra depression suggest a link to active structures during the

Table 1. LR model by restoration step curvature

Curvature at Restoration Step	Model Parameters	Estimate	Std. Error	z Value	Pr(> z)
Cretaceous	Intercept	-2.1238	0.0126	-168.51	0.0000
	K_1 Coefficient	1.8593	0.1397	13.31	0.0000
Jurassic	Intercept	-2.1284	0.0125	-170.37	0.0000
	K_2 Coefficient	2.3498	0.1630	14.42	0.0000
Triassic	Intercept	-2.2602	0.0131	-172.59	0.0000
	K_3 Coefficient	3.6023	0.1147	31.40	0.0000
Upper Permian	Intercept	-2.3008	0.0132	-174.76	0.0000
	K_4 Coefficient	4.4837	0.1196	37.48	0.0000

The z-values with the associated p-values correspond to Wald z-statistic. The resulting p-values indicate that the null-hypothesis can be rejected, and therefore each predictor individually is statistically significant in the predictive model for Cu-potentials (for more details about the significance test of predictors see Hosmer and Lemeshow 2004)

Table 2. LR model by complementary predictors

Complementary Predictors	Model Parameters	Estimate	Std. Error	z Value	Pr(> z)
HBF	Intercept	-1.5656	0.0188	-83.17	0.0000
	Coefficient	-0.0092	0.0003	-27.44	0.0000
ZBK	Intercept	-1.4691	0.0508	-28.90	0.0000
	Coefficient	-0.1360	0.0122	-11.19	0.0000

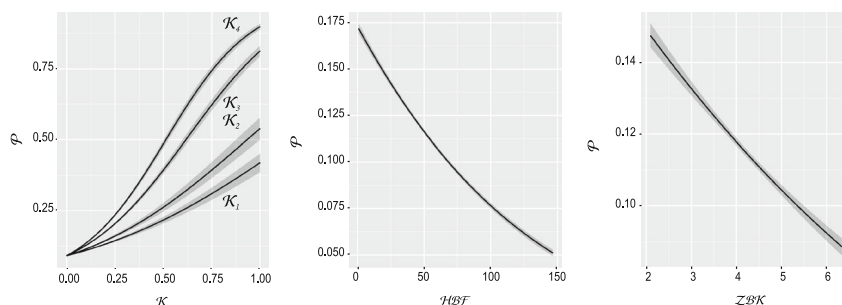


Fig. 8. Predicted probabilities from the LR models by predictor. Each image corresponds to the predicted probability of having a Cu-potential location according to the predictor individually (*HFB* and *ZBK* in km).

Triassic and Jurassic and less strongly during the Cretaceous (Fig. 7d, c and b). Finally, the Cretaceous restoration indicates a relationship between the fault systems of Sieroszowice graben with proximal potential areas for this period (Fig. 7a and 10).

Several attempts have been made to determine the age of the Kupferschiefer mineralization (Jowett et al. 1987; Bechtel et al. 1999; Michalik 1997). The wide range of different ages obtained in those and similar works (from Late Permian to Late Jurassic) have been explained in terms of multi-stage mineralization (Speczik 1995). The curvature obtained at

each time-restoration step reveals a strong spatial correlation between high curvature values and Cu-potentials. This association between high curvature and Cu-mineralization/enrichment could help in understanding of timing and structural mechanisms involved in ore formation. Table 4 presents synthetically the geodynamic setting, the dominant tectonic process that occurred in the region and the Cu-potential areas with high curvature values for each restoration. The method exposed in this work may improve metallogenic models for this kind of ore-deposit, relating geodynamic evolution, fluid pathways, and mineralized areas.

DISCUSSION

In this work we model horizons overlying the Zechstein Formation as continuous surfaces,

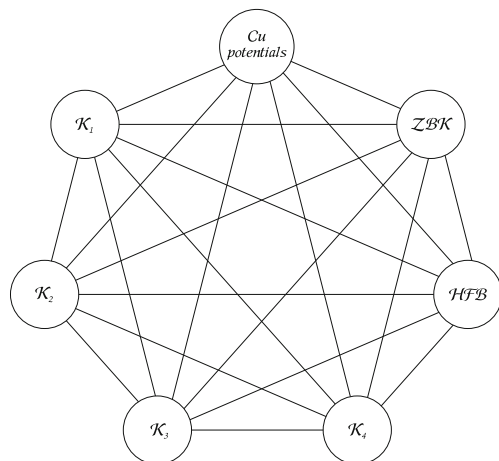


Fig. 9. Graph of the conditional independence test for K_l ($l = 1$: Cretaceous, 2: Jurassic, 3: Triassic, 4: Upper Permian), HFB and ZBK given Cu-potentials. Each arc represents the lack of the conditional independence for the predictors in the corresponding nodes. For the test we used the *bnlearn-R* package (for more details about the conditional independence test see Scutari 2010).

assuming that the different tectonic events that occurred before the Alpine orogeny have caused folding rather than faulting in these horizons. The resulting surface geometry depends on the interpretive points used as input data for the 3D modeling, on the way interpolation is done between these points and on the mesh resolution used to model the surface. All three elements are potential sources of uncertainty and inaccuracy in the final structural geometry, which could possibly affect the potential mapping results. More precisely, we used discrete smooth interpolation (DSI) (Mallet 2002) for creating these continuous triangulated surfaces. In DSI, the nodes of the triangular mesh are placed so as to minimize data misfit and roughness (Laplacian). Given the data spacing and the chosen surface resolution, the interpolation error due to smoothing is considered minimal. The error due to the limited surface mesh resolution is likely more significant in high-curvature areas. Therefore, the detection of fault activity using curvature analysis may be under-estimated due to the limited surface mesh resolution. In the final potential map, this means that basement faults having a slight displacement may remain undetected due to negligible curvature in the overlying horizons. This effect could easily be mitigated by refining the mesh in the neighborhood of the faults (Caumon et al. 2009).

Table 3. LR model coefficients with interaction terms

	Estimate	Std. Error	z Value	Pr(> z)
(Intercept)	-9.6360	0.2061	-46.74	0.0000
K_1	57.9567	2.6291	22.04	0.0000
K_2	-154.8190	6.9061	-22.42	0.0000
K_3	101.7225	4.2253	24.07	0.0000
K_4	60.7357	2.2193	27.37	0.0000
HFB	-0.1236	0.0030	-40.89	0.0000
ZBK	2.6126	0.0560	46.62	0.0000
HFB*ZBK	0.0100	0.0005	20.36	0.0000
$K_1 * K_2$	38.3345	6.0877	6.30	0.0000
$K_1 * K_3$	-35.0253	5.4303	-6.45	0.0000
$K_1 * K_4$	-31.4186	2.7922	-11.25	0.0000
$K_1 * HFB$	0.4292	0.0262	16.36	0.0000
$K_1 * ZBK$	-19.2036	0.8572	-22.40	0.0000
$K_2 * K_3$	-16.2740	3.0681	-5.30	0.0000
$K_2 * K_4$	27.5323	6.4375	4.28	0.0000
$K_2 * HFB$	-0.8229	0.0576	-14.29	0.0000
$K_2 * ZBK$	44.2964	2.0726	21.37	0.0000
$K_3 * K_4$	-38.5078	4.1089	-9.37	0.0000
$K_3 * HFB$	0.5444	0.0389	14.01	0.0000
$K_3 * ZBK$	-28.3073	1.3762	-20.57	0.0000
$K_4 * HFB$	0.5212	0.0246	21.22	0.0000
$K_4 * ZBK$	-18.9501	0.7905	-23.97	0.0000

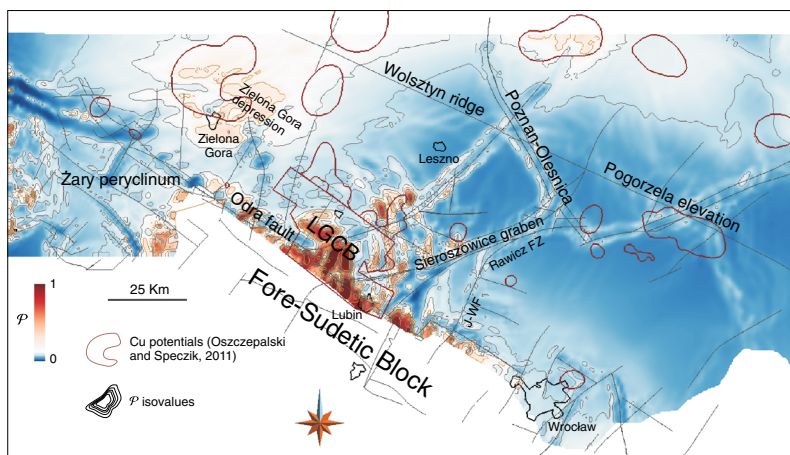


Fig. 10. Predicted probabilities of Cu-potentials (P) in the FSM. Some main structures and Cu potential locations are highlighted. The match between high P and the Cu-potential areas are close to main regional structures as the Pogorzela elevation, the Sieroszowice graben and the Odra fault system among others.

Table 4. Restoration steps, geodynamic setting, and high curvature in Cu-potential areas

Restoration Step	Tectonic Process	Geodynamic Setting	Cu-Potential Area ^a
Upper Permian	Ending tectono-magmatic pulses. Rapid subsidence	Ending Variscan orogeny. Opening Tethys sea	Luboszyce, Scinawa, Czeklin, Kózuchów, Kaleje, LGCB
Triassic	Subsidence, extensional tectonics	Rifting phase	Luboszyce, Czeklin, Słubów, Zarków, Mozów, Wilcze, LGCB
Jurassic	Increasing subsidence rates, extensional tectonics. Late Jurassic uplift	Arctic–North Atlantic rifting. Late Jurassic basin inversion	Luboszyce, Scinawa Czeklin, Zarków, Mozów, LGCB
Cretaceous	Uplift	Alpine-related basin inversion	Janowo, Kózuchów Milicz, Sułmierzyce, Słubów Zarków, Kaleje, Mozów, LGCB

^aAccording to Oszczepalski and Speczik (2011)

We nonetheless chose a constant resolution to avoid overfitting effects. Indeed, we believe the main source of uncertainty in the results stems from the depth maps and interpreted seismic sections used for the structural modeling. The geometry of these “data” and of the associated fault locations is well constrained close to boreholes but is obviously more uncertain in sparsely drilled areas. Structural uncertainty assessment methods (Wellmann et al. 2010; Cherpeau et al. 2010) could be used to address these sources of uncertainty. In the present study, we consider that bias due to possible interpretation errors may be present in areas with low borehole density, especially in the NE and SE parts of the study area (Fig. 2b).

The map of predicted probabilities for Cu-potential areas using curvature values with interaction terms (Fig. 10) shows several regions with medium to high potentials. The predictive model applied to obtain this map only considers geometric parameters relating fault systems that may have played a role with the Kupferschiefer formation. However, the Kupferschiefer ore creation has involved other factors such as passage of metalliferous fluids (Oszczepalski 1999), amount of organic matter in the Kupferschiefer Formation (Bechtel et al. 2001; Gouin 2008) and the presence of meteoric recharge systems (Brown 2011), among others. In this sense, a predictive model accounting only for structural parameters is incomplete. Future work could, thus,

consider these other sources of information as additional predictors (if they can be extrapolated with limited uncertainties) or as a means to locally test the predictability of the proposed potential model.

CONCLUSIONS

Curvature from the FSM restorations are related spatially with the Cu-potential areas established in previous works. This relation probably expresses the impact of fault systems active during the mineralization process. Upward migration of thermal fluids along deep faults and damaged areas in the rocks mass could directly influence the Cu-sulfides formation. The Cu distribution patterns in the FSM were caused by variation of the stress regime during the tectonic evolution from Late Permian to Late Cretaceous. The Odra fault system has controlled the mineralization at Late Permian times, but during the Triassic and Jurassic other fault-systems ruled the mineralization, especially the faults related to the Pogorzela elevation, the Sieroszowice graben and the Zielona Góra depression.

The utility of curvature as a predictor is evidenced from the LR analysis, completing the set of structural parameters also obtained from the restoration modeling. We believe that the above ideas and methods can be applied in similar cases where fault systems are sealed by an impermeable cap and the occurrence of hot brines expulsion events from the basement.

ACKNOWLEDGMENTS

This work has been performed in the frame of the Gocad research project. We thank the industry and academic members of the Gocad Research Consortium (<http://www.gocad.org/w4/index.php/consortium/members>) for supporting this research. We thank Paradigm for the Gocad software. We appreciate the collaboration of Clementine Fourrier (Université de Lorraine). We thank Piotr Krzemiński (Mozów Copper SP z o.o.) for his comments and remarks which helped improve this paper. Finally, our special thanks go to Laurent Ailleres (Monash University) and Tobias Bauer (Luleå University of Technology) for very helpful observations and discussions. Part of this research received funding from the European Union's Seventh Framework Program under grant agreement

n°228559 (ProMine Project), and was performed in the framework of the of Investissements d'avenir **Labex RESSOURCES21** (ANR-10-LABX-21).

REFERENCES

- Agterberg, F., Bonham-Carter, G., Cheng, Q., & Wright, D. (1993). Weights of evidence modeling and weighted logistic regression for mineral potential mapping. In *Proceedings of the Computers in Geology-25 Years of Progress* (pp. 13–32). Oxford: Oxford University Press Inc.
- Bechtel, A., Elliott, W. C., Wampler, J. M., & Oszczeplski, S. (1999). Clay mineralogy, crystallinity, and K-Ar ages of illites within the Polish Zechstein basin; implications for the age of Kupferschiefer mineralization. *Economic Geology*, 94, 261–272.
- Bechtel, A., Gratzner, R., Püttmann, W., & Oszczeplski, S. (2001). Variable alteration of organic matter in relation to metal zoning at the Rote Fäule front (Lubin-Sieroszowice mining district, SW Poland). *Organic Geochemistry*, 32(3), 377–395.
- Blundell, D. J., Karnkowski, P. H., Alderton, D. H. M., Oszczeplski, S., & Kucha, H. (2003). Copper mineralization of the Polish Kupferschiefer: A proposed basement fault-fracture system of fluid flow. *Economic Geology*, 98(7), 1487–1495.
- Bond, C., Gibbs, A., Shipton, Z., & Jones, S. (2007). What do you think this is? “Conceptual uncertainty” in geoscience interpretation. *GSA Today*, 17(11), 4–10.
- Botella, A., Lévy, B., & Caumon, G. (2013). Indirect hex-dominant mesh generation using a matching tetrahedra method. In *Proceedings of the 33rd Gocad Meeting*. Nancy: ASGA.
- Brown, A. C. (2011). Adding geochemical rigor to the general basin-scale genetic model for sediment-hosted stratiform copper mineralization. In *Proceedings of the 11th SGA Biennial Meeting*. Antofagasta: SGA.
- Caumon, G. (2010). Towards stochastic time-varying geological modeling. *Mathematical Geosciences*, 42(5), 555–569.
- Caumon, G., Collon-Drouaillet, P., Carlier, Le, de Veslud, C., Viseur, S., & Sausse, J. (2009). Surface-based 3D modeling of geological structures. *Mathematical Geosciences*, 41, 927–945.
- Chamberlin, R. T. (1910). The Appalachian folds of central Pennsylvania. *The Journal of Geology*, 18(3), 228–251.
- Cheng, Q. (2008). Non-linear theory and power-law models for information integration and mineral resources quantitative assessments. In *Progress in Geomathematics*, (pp. 195–225). Berlin: Springer.
- Cherpeau, N., Caumon, G., & Lévy, B. (2010). Stochastic simulations of fault networks in 3D structural modeling. *Comptes Rendus Geoscience*, 342(9), 687–694.
- Dadlez, R., Marek, S., & Pokorski, J. (2000). *Geological map of Poland without Cainozoic deposits*. Warszawa: Państwowy Instytut Geologiczny.
- Dahlstrom, C. (1969). Balanced cross sections. *Canadian Journal of Earth Sciences*, 6(4), 743–757.
- de Araújo, C. C., & Macedo, A. B. (2002). Multicriteria geologic data analysis for mineral favorability mapping: Application to a metal sulphide mineralized area, Ribeira valley metallogenic province Brazil. *Natural Resources Research*, 11, 29–43.
- de Quadros, T., Koppe, J., Strieder, A., & Costa, J. (2006). Mineral-potential mapping: A comparison of weights-of-evidence and fuzzy methods. *Natural Resources Research*, 15(1), 49–65.
- De Santi, M., Campos, J., & Martha, L. (2002). A finite element approach for geological section reconstruction. In *Proceedings of the 22th Gocad Meeting*. Nancy: ASGA.

- Duffy, O. B., Gawthorpe, R. L., Docherty, M., & Brocklehurst, S. H. (2013). Mobile evaporite controls on the structural style and evolution of rift basins: Danish Central Graben North Sea. *Basin Research*, 25(3), 310–330.
- Durand-Riard, P., Caumon, G., & Muron, P. (2010). Balanced restoration of geological volumes with relaxed meshing constraints. *Computers & Geosciences*, 36, 441–452.
- Durand-Riard, P., Guzowski, C. A., Caumon, G., & Titeux, M. O. (2013). Handling natural complexity in 3D geomechanical restoration, with application to the recent evolution of the outer fold-and-thrust belt, deepwater Niger Delta. *AAPG Bulletin*, 97(1), 87–102.
- Finch, E., Hardy, S., & Gawthorpe, R. (2004). Discrete-element modelling of extensional fault-propagation folding above rigid basement fault blocks. *Basin Research*, 16(4), 467–488.
- Forster, C., & Smith, L. (1989). The influence of groundwater flow on thermal regimes in mountainous terrain: A model study. *Journal of Geophysical Research: Solid Earth (1978–2012)*, 94(B7), 9439–9451.
- Gao, D. (2013). Integrating 3D seismic curvature and curvature gradient attributes for fracture characterization: Methodologies and interpretational implications. *Geophysics*, 78(2), O21–O31.
- Gouin, J. (2008). Mode de genèse et valorisation des minerais de type black shales: cas du Kupferschiefer (Pologne) et des schistes noirs de Talvivaara (Finlande). Ph.D. thesis report, Université d'Orléans, Orléans.
- Gratier, J. P., & Guillier, B. (1993). Compatibility constraints on folded and faulted strata and calculation of total displacement using computational restoration (UNFOLD program). *Journal of structural geology*, 15(3), 391–402.
- Groshong, R. (2006). *3-D structural geology. A practical guide to quantitative surface and subsurface map interpretation* (2nd ed.). Berlin Heidelberg: Springer-Verlag.
- Guzowski, C., Mueller, J., Shaw, J., Muron, P., Medwedeff, D., Bilotti, F., et al. (2009). Insights into the mechanisms of fault-related folding provided by volumetric structural restorations using spatially varying mechanical constraints. *AAPG Bulletin*, 93, 479–502.
- Hitzman, M. W., Selley, D., & Bull, S. (2010). Formation of sedimentary rock-hosted stratiform copper deposits through Earth history. *Economic Geology*, 105(3), 627–639.
- Hosmer, D. W., Jr, & Lemeshow, S. (2004). *Applied logistic regression*. London: John Wiley.
- Jarvis, A., Reuter, H., Nelson, A., & Guevara, E. (2008). *Hole-filled SRTM for the globe version 4*. Retrieved from the CGIAR-SXI SRTM 90m database <http://srtm.csicgiar.org>.
- Jowett, E. C. (1986). Genesis of Kupferschiefer Cu-Ag deposits by convective flow of Rotliegendes brines during triassic rifting. *Economic Geology*, 81(8), 1823–1837.
- Jowett, E. C., Pearce, G. W., & Rydzewski, A. (1987). A mid-Triassic paleomagnetic age of the Kupferschiefer mineralization in Poland, based on a revised apparent polar wander path for Europe and Russia. *Journal of Geophysical Research*, 92(B1), 581–598.
- Kane, K. E., Jackson, C. A. L., & Larsen, E. (2010). Normal fault growth and fault-related folding in a salt-influenced rift basin: South Viking Graben, offshore Norway. *Journal of Structural Geology*, 32(4), 490–506.
- Karmkowski, P. H. (1999). Origin and evolution of the polish Rotliegend basin. *Polish Geological Institute Special Papers*, 3, 1–93.
- Kerrick, R. (1993). Perspectives on genetic models for lode gold deposits. *Mineralium Deposita*, 28(6), 362–365.
- KGHM Polska Miedź, S. A. (2012). Report on the mining assets of KGHM Polska Miedź S.A. located within the Legnica-Głogów Copper Belt Area. Report prepared by an internal team of KGHM Polska Miedź S. A. 50, KGHM Polska Miedź S.A., Poland.
- Krzywiec, P. (2006). Triassic–Jurassic evolution of the pomeranian segment of the Mid-Polish Trough: Basement tectonics and subsidence patterns. *Geological Quarterly*, 50, 139–150.
- Lecour, M., Cognot, R., Duvinage, I., Thore, P., & Dulac, J. C. (2001). Modelling of stochastic faults and fault networks in a structural uncertainty study. *Petroleum Geoscience*, 7(S), S31–S42.
- Lefebvre, J. (1989). Les gisements stratiformes en roche sédimentaire d'Europe centrale (Kupferschiefer) et de la Ceinture Cuprifère du Zaïre et de Zambie. *Annales de la Société Géologique de Belgique*, 112(1), 121–135.
- Lisle, R. (1994). Detection of zones of abnormal strains in structures using Gaussian curvature analysis. *AAPG Bulletin*, 78(12), 1811–1819.
- Maerten, L., & Maerten, F. (2006). Chronologic modeling of faulted and fractured reservoirs using geomechanically based restoration: Technique and industry applications. *AAPG Bulletin*, 90(8), 1201–1226.
- Mallet, J. L. (2002). *Geomodeling*. Oxford: Oxford University Press.
- Mazur, S., Scheck-Wenderoth, M., & Krzywiec, P. (2005). Different modes of the Late Cretaceous – Early Tertiary inversion in the North German and Polish basins. *International Journal of Earth Sciences*, 94(5), 782–798.
- Mazur, S., Aleksandrowski, P., Turniak, K., Krzemiński, L., Mastalerz, K., Górecka-Nowak, A., et al. (2010). Uplift and late orogenic deformation of the Central European Variscan belt as revealed by sediment provenance and structural record in the Carboniferous foreland basin of western Poland. *International Journal of Earth Sciences*, 99(1), 47–64.
- McCullagh, P., & Nelder, J. A. (1989). *Generalized linear models (monographs on statistics and applied probability 37)*. London: Chapman Hall.
- Mejia, P., & Royer, J. J. (2012). Explicit surface restoring-decompacting procedure to estimate the hydraulic fracturing: Case of the Kupferschiefer in the Lubin region, Poland. In *Proceedings of the 32nd Gocad Meeting*. Nancy: ASGA.
- Michalik, M. (1997). *Mineral deposits, research and exploration. Chlorine containing illites, copper chlorides and other chloride bearing minerals in the fore-sudetic copper deposit (Poland)* (pp. 543–546). Rotterdam: Balkema.
- Moretti, I. (2008). Working in complex areas: New restoration workflow based on quality control, 2D and 3D restorations. *Marine and Petroleum Geology*, 25(3), 205–218.
- Moretti, I., Lepage, F., & Guiton, M. (2006). KINE3D: a new 3D restoration method based on a mixed approach linking geometry and geomechanics. *Oil & Gas Science and Technology - Revue d'IFP Energies nouvelles*, 61(2), 277–289.
- Moretti, I., Delos, V., Letouzey, J., Otero, A., & Calvo, J. C. (2007). The use of surface restoration in foothills exploration: Theory and application to the sub-Andean zone of Bolivia. In O. Lacombe, F. Roure, J. Lavé, & J. Vergés (Eds.), *Thrust belts and foreland basins, frontiers in earth sciences* (pp. 149–162). Berlin Heidelberg: Springer.
- Muchez, P., Heijlen, W., Banks, D., Blundell, D., Boni, M., & Grandia, F. (2005). 7: Extensional tectonics and the timing and formation of basin-hosted deposits in Europe. *Ore Geology Reviews*, 27(1), 241–267.
- Narkiewicz, M., Resak, M., Littke, R., & Marynowski, L. (2010). New constraints on the middle palaeozoic to cenozoic burial and thermal history of the holy cross mts. Central Poland: Results from numerical modelling. *Geologica Acta*, 8, 189–205.
- Oszczepalski, S. (1999). Origin of the Kupferschiefer polymetallic mineralization in Poland. *Mineralium Deposita*, 34, 599–613.
- Oszczepalski, S., & Speczik, S. (2011). Prospectivity analysis of the polish Kupferschiefer: New insight. In *Proceedings of the 11th SGA Biennial Meeting*. Antofagasta: SGA.

- Oszczepalski, S., Rydzewski, A., & Geologiczny, I. (1997). *Met-allogenic atlas of Zechstein copper-bearing series in Poland*. Wydawnictwo Kartograficzne Polskiej Agencji Ekologicznej.
- PARADIGM. (2012). *Training guide: modeling reservoir architecture*. SKUA—Paradigm. PARADIGM.
- Pawlak, W., Aniol-Kwiatkowska, J., Pawlak, J., Nowak-Ferdhus, E., Migoń, P., & Malicka, A. et al. (2008). *Atlas Śląska Dolnego i Opolskiego*. Uniwersytet Wrocławski. Pracownia Atlasu Dolnego Śląska.
- Pieczonka, J., Piestrzyński, A., Mucha, J., Głuszek, A., Kotarba, M., & Wieclaw, D. (2008). The red-bed-type precious metal deposit in the Sieroszowice–Polkowice copper mining district, SW Poland. *Annales Societatis Geologorum Poloniae*, 78, 151–280.
- Piesterzyński, A., Pieczonka, J., & Głuszek, A. (2002). Redbed-type gold mineralisation, Kupferschiefer, south-west Poland. *Mineralium Deposita*, 37(5), 512–528.
- Rentzsch, J., & Franzke, H. (1997). Regional tectonic control of the Kupferschiefer mineralization in Central Europe. *Zeitschrift für Geologische Wissenschaften*, 25, 141–150.
- Rentzsch, J., Franzke, H., & Friedrich, G. (1997). Die laterale Verbreitung der Erzmineralassoziationen im deutschen Kupferschiefer. *Zeitschrift für Geologische Wissenschaften*, 25, 121–140.
- Resak, M., Narkiewicz, M., & Littke, R. (2008). New basin modelling results from the Polish part of the Central European Basin system: Implications for the late cretaceous—early paleogene structural inversion. *International Journal of Earth Sciences*, 97(5), 955–972.
- Roberts, A. (2001). Curvature attributes and their application to 3D interpreted horizons. *First Break*, 19(2), 85–100.
- Rouby, D. (1994). *Restauration en carte des domaines failés en extension. Méthode et applications*. PhD thesis, Université Rennes 1.
- Schaeben, H. (2012). Comparison of mathematical methods of potential modeling. *Mathematical Geosciences*, 44, 101–129.
- Schaeben, H. (2013). Bits of mathematics of potential modelling. In *Proceedings of the 12th Biennial SGA Meeting on Mineral Deposits Research for a High-Tech World*, (vol. 2, pp. 489–491). Uppsala: SGA.
- Schaeben, H. (2014). Potential modeling: Conditional independence matters. *GEM—International Journal on Geomathematics*, 5(1), 99–116.
- Schaeben, H., & Schmidt, S. (2013). Theoretical and practical comparison of weights-of-evidence and logistic regression models based on the notion of Markov random fields. In *Proceedings of the 33rd Gocad Meeting*. Nancy: ASGA.
- Scheck-Wenderoth, M., & Lamarche, J. (2005). Crustal memory and basin evolution in the Central European Basin system: New insights from a 3D structural model. *Tectonophysics*, 397(1–2), 143–165.
- Schmidt Mumm, A., & Wolfgramm, M. (2004). Fluid systems and mineralization in the north German and Polish basins. *Geofluids*, 4(4), 315–328.
- Sclater, J. G., & Christie, P. A. F. (1980). Continental stretching: An explanation of the post-mid-cretaceous subsidence of the Central North Sea basin. *Journal of Geophysical Research*, 85(B7), 3711–3739.
- Scutari, M. (2010). Learning Bayesian networks with the bnlearn R package. *Journal of Statistical Software*, 35(3), 1–22.
- Speczik, S. (1995). The Kupferschiefer mineralization of Central Europe: New aspects and major areas of future research. *Ore Geology Reviews*, 9(5), 411–426.
- Speczik, S., Oszczepalski, S., Karwasiecka, M., & Nowak, G. (2007). Kupferschiefer: A hunt for new reserves. In *Proceedings of the 9th Biennial SGA Meeting on Digging Deeper* (pp. 237–240). Dublin: Irish Association for Economic Geology.
- Stephenson, R. A., Narkiewicz, M., van Dadlez, R., Wees, J. D., & Andriessen, P. (2003). Tectonic subsidence modelling of the Polish basin in the light of new data on crustal structure and magnitude of inversion. *Sedimentary Geology*, 156, 59–70.
- Symons, D., Kawasaki, K., Walther, S., & Borg, G. (2011). Paleomagnetism of the Cu-Zn-Pb-bearing Kupferschiefer black shale (Upper Permian) at Sangerhausen Germany. *Mineralium Deposita*, 46(2), 137–152.
- Titeux, M. O. (2009). *Restauration et incertitudes structurales: Changement d'échelles des propriétés mécaniques et gestion de la tectonique salifère*. PhD thesis, Institut National Polytechnique de Lorraine.
- Vaughan, D. J., Sweeney, M. A., Friedrich, G., Diedel, R., & Hararczyk, C. (1989). The Kupferschiefer: An overview with an appraisal of the different types of mineralization. *Economic Geology*, 84(5), 1003–1027.
- Verrall, P. (1981). Structural interpretation with application to North Sea problems. Course note no. 3. Joint Association for Petroleum Exploration courses (UK).
- Vidal-Royo, O., Cardozo, N., Muoz, J. A., Hardy, S., & Maerten, L. (2012). Multiple mechanisms driving detachment folding as deduced from 3D reconstruction and geomechanical restoration: the Pico del Águila anticline (External Sierras, southern Pyrenees). *Basin Research*, 24(3), 295–313.
- Wagner, T., Okrusch, M., Weyer, S., Lorenz, J., Lahaye, Y., Taubald, H., et al. (2010). The role of the Kupferschiefer in the formation of hydrothermal base metal mineralization in the Spessart ore district, Germany: insight from detailed sulfur isotope studies. *Mineralium Deposita*, 45(3), 217–239.
- Wedepohl, K., & Rentzsch, J. (2006). The composition of brines in the early diagenetic mineralization of the Permian Kupferschiefer in Germany. *Contributions to Mineralogy and Petrology*, 152(3), 323–333.
- Wellmann, J. F., Horowitz, F. G., Schill, E., & Regenauer-Lieb, K. (2010). Towards incorporating uncertainty of structural data in 3D geological inversion. *Tectonophysics*, 490(34), 141–151.
- Withjack, M. O., & Callaway, S. (2000). Active normal faulting beneath a salt layer: an experimental study of deformation patterns in the cover sequence. *AAPG Bulletin*, 84, 627–651.
- Withjack, M. O., Olson, J., & Peterson, E. (1990). Experimental models of extensional forced folds (1). *AAPG Bulletin*, 74, 1038–1054.
- Wodzicki, A., & Piestrzyński, A. (1994). An ore genetic model for the Lubin–Sieroszowice mining district Poland. *Mineralium Deposita*, 29(1), 30–43.
- Ziegler, P. (1982). *Geological atlas of Western and Central Europe*. Singapore: Shell International Petroleum Maatschappij B.V.
- Zuo, R., & Carranza, E. J. M. (2011). Support vector machine: A tool for mapping mineral prospectivity. *Computers & Geosciences*, 37(12), 1967–1975.